The PRIMA promise of deciphering interstellar dust evolution with observations of the nearby Universe

Frédéric GALLIANO[a,*], Maarten BAES[b], Léo BELLOIR[a], Simone BIANCHI[c], Caroline BOT[d], Francesco CALURA[e], Viviana CASASOLA[e], Jérémy CHASTENET[b], Christopher CLARK[f], Lucie CORREIA[d], Ilse DE LOOZE[b], Mika JUVELA[g], Hidehiro KANEDA[h], Stavroula KATSIOLI[i], Francisca KEMPER[j,k,l], Vianney LEBOUTEILLER[a], Suzanne MADDEN[a], Mikako MATSUURA[m], Takashi ONAKA[n], Lara PANTONI[b], Francesca POZZI[e], Monica RELAÑO PASTOR[o], Marc SAUVAGE[a], Matthew SMITH[m], Vidhi TAILOR[e], Tsutomu T. TAKEUCHI[p,q], Emmanuel XILOURIS[i], Nathalie YSARD[r]

[a]Université Paris-Saclay, Université Paris Cité, CEA, CNRS, AIM, 91191, Gif-sur-Yvette, France
[b]Sterrenkundig Observatorium, Universiteit Gent, Krijgslaan 281 S9, B-9000 Gent, Belgium
[c]INAF-Osservatorio Astrofisico di Arcetri, L. E. Fermi 5, 50125 Firenze, Italy
[d]Université de Strasbourg, CNRS, Observatoire astronomique de Strasbourg, UMR 7550, F-67000 Strasbourg, France
[e]INAF – Istituto di Radioastronomia, Via P. Gobetti 101, 40129 Bologna, Italy
[f]Space Telescope Science Institute, 3700 San Martin Drive, Baltimore, MD 21218-2463, USA
[g]Department of Physics, PO Box 64, University of Helsinki, 00014 Helsinki, Finland
[h]Graduate School of Science, Nagoya University, Furo-cho, Chikusa-ku, Nagoya 464-8602, Japan
[i]National Observatory of Athens, IAASARS, GR-15236, Athens, Greece
[j]Institute of Space Sciences (ICE), CSIC, Can Magrans, 08193 Cerdanyola del Vallés, Barcelona, Spain
[k]ICREA, Pg. Lluís Companys 23, Barcelona, Spain
[l]Institut d'Estudis Espacials de Catalunya (IEEC), E-08034 Barcelona, Spain
[m]School of Physics and Astronomy, Cardiff University, The Parade, Cardiff CF24 3AA, UK
[n]Department of Astronomy, Graduate School of Science, University of Tokyo, 7-3-1 Hongo, Bunkyo-ku, Tokyo 113-0033, Japan
[o]Dept. Física Teórica y del Cosmos, Universidad de Granada, Spain
[p]Division of Particle and Astrophysical Science, Nagoya University, Furo-cho, Chikusa-ku, Nagoya 464-8602, Japan
[q]The Research Center for Statistical Machine Learning, the Institute of Statistical Mathematics, 10–3 Midori-cho, Tachikawa, Tokyo 190–8562, Japan
[r]IRAP, Université de Toulouse, CNRS, UPS, IRAP, Toulouse Cedex 4, France

Abstract. This paper develops a few science cases, using the PRIMA far-IR probe, aimed at achieving several breakthroughs in our understanding of the dust properties and their evolution. We argue that the specific observational capabilities of PRIMA, namely its unprecedented sensitivity over the whole far-IR range and the possibility to obtain continuous spectra between $\lambda = 24$ and $235\ \mu$m, are essential to progress in our understanding of the physics of the interstellar medium and galaxy evolution. Our science cases revolve around observations of nearby galaxies. We discuss the importance of detecting the IR emission of the diffuse interstellar medium of these galaxies, including very low-metallicity systems. We also discuss the opportunity of detecting various solid-state features to understand the mineralogy of interstellar grains. Finally, we stress the unique opportunity brought by the possible simultaneous measures of both the dust continuum and the far-IR fine-structure gas lines. These science cases could be distributed in a few large programs.

Keywords: Infrared, interstellar medium, dust, galaxies, dwarf galaxies.

*Frédéric GALLIANO, frederic.galliano@cea.fr

1 Introduction

Dust grains are a crucial ingredient of the physics of the *InterStellar Medium* (ISM), obscuring starlight, heating the neutral gas, and catalyzing numerous prominent chemical reactions.[1] Dust observables also provide invaluable diagnostics of the physical conditions from Galactic clouds to high redshift galaxies, allowing the observer to derive *Star Formation Rates* (SFR), dust and gas masses, the magnetic field orientation, *etc.* The knowledge of interstellar dust physics is thus necessary for understanding both galaxy evolution[2] and the process of star formation, down to the formation of planetary systems[3] and prebiotic chemistry.[4] This knowledge is unfortunately hampered by large uncertainties. First, the precise dust constitution (chemical composition, structure, size and shape distributions) in a given region is extremely difficult to infer, due to degeneracies between the optical properties and the size distribution. In addition, the grain properties are known to evolve with the density and UV field, in the *Milky Way* (MW).[5] Dust observables from the UV to the microwave regime exhibit complex dependencies when spatially resolved at scales of interstellar clouds.[6–10] Outside the MW, these parameters are also important, but the abundance of elements heavier than Helium, the *metallicity*, which is quite uniform in the MW, appears to be the main quantity shaping the dust observables of galaxies of different types [11–13].

Our current poor knowledge of the dust properties and their evolution is thus an obstacle to answering fundamental questions in astrophysics. For instance, the dust-to-gas mass ratio of galaxies as a function of their metallicity, a relation essential to quantifying the balance between dust formation and destruction, differs significantly in the low-metallicity regime if it is measured using the thermal emission observed in the *Far-InfraRed* (FIR) or using elemental depletions from UV absorption lines.[14–16] This discrepancy might be linked to both our lack of knowledge of the FIR opacity of grain mixtures at low metallicity, and to biases of the depletion method. Another example of the limitations we face is the so-called *submillimeter (submm) excess*, a systematic deviation between the submm-mm observations and contemporary state-of-the art models [17–23]. This excess is more prominent at low metallicity and potentially biases dust mass estimates. Finally, the UV-to-FIR extinction law also depends on the environment. Its environmental variation is relatively well-known in the MW, from an empirical point of view,[24,25] although its interpretation in terms of variation of the grain constitution is still debated. However, outside the MW, our knowledge of the extinction curve is limited to a handful of sightlines in the most nearby galaxies, primarily the Magellanic Clouds.[8,10] The Magellanic extinction curves do not resemble those of the MW. Magellanic extinction curves are sometimes used to unredden observations of galaxies without any rigorous justification. This potentially induces systematic effects in all the UV-to-mid-IR (UV-to-MIR) tracers.

Ab initio simulations of the formation and evolution of interstellar grains are not yet feasible.[26] We thus essentially rely on an empirical approach, complemented by our knowledge of solid-state physics. There are several observational clues that we would need to obtain to move forward. First, contemporary dust models are solely constrained by the IR *Spectral Energy Distribution* (SED), the UV-to-MIR extinction curve, the elemental depletions and the polarization fraction in extinction and emission of the diffuse ISM of the MW.[27,28] This heterogeneous set of constraints is required to solve the degeneracies between the optical properties and the size distribution.[1] We thus lack an extragalactic dust model that could account for the effects of metallicity, as well as those of the density and UV field. Ideally, we would need similar sets of constraints in the diffuse ISM of external galaxies, starting with the Magellanic clouds, to thoroughly understand the effect of metallicity. In addition, we would need a way to quantify the evolution of the diffuse ISM dust mixture into denser and more illuminated regions, where these observables are more difficult to obtain and more ambiguous to interpret due to the mixing of physical conditions along the sightline. Second, the low-metallicity regime is crucial to understanding the early stages of dust formation and inferring what happens in primordial galaxies.[29] Low-metallicity systems have been studied with *Herschel*,[12,30–33] but we lack statistics at *extremely* low metallicity ($Z \lesssim 1/10\ Z_\odot$) and at quiescent star-formation activities. Finally, MIR solid-state features in emission or absorption are instrumental in characterizing accurate stoichiometry and structure of the material constituting the grains. JWST, after ISO and *Spitzer*, is currently detecting numerous such features, but it is spectrally limited to the range where they are mixed with the bright features coming from *Polycyclic Aromatic Hydrocarbons* (PAHs). Yet, there are numerous features longward of $\lambda = 28\ \mu$m that would allow us to better characterize the grain composition. PRIMA offers the promise to address several of these issues, thanks to its unmatched sensitivity in the FIR, its continuous-wavelength spectroscopic capability, and its polychromatic polarization imager.[34,35]

The present paper proposes ways to address the limitations listed above using PRIMA observations of nearby galaxies. We focus our discussion on what PRIMA data will bring to our science questions. However, most of our targets have been fully mapped with *Spitzer* and some are currently being imaged with the JWST. These mid-IR data will be instrumental in completing PRIMA's spectral coverage at short wavelengths. In Sect. 2, we argue for the necessity to obtain deep observations of the diffuse ISM of the Magellanic Clouds. We then discuss the constraints on interstellar grain mineralogy accessible with PRIMA, in Sect. 3. The degeneracy between the effects of metallicity and star-formation activity, and a way to solve it, is presented in Sect. 4. Finally, Sect. 5 proposes a way of combining dust and gas tracers to better understand the grain properties of dense, UV-illuminated regions. We end with a conclusion in Sect. 6. Throughout this paper, we use *The Heterogenous dust Evolution Model for Interstellar Solids* (`THEMIS`)[36] as a reference. All the figures and flux estimates are done using this model. Our observing strategy is based on the formulae summarized in Appendix A.

2 Unveiling the Elusive Dust Properties of the Diffuse ISM of Nearby Galaxies

We have stated in Sect. 1 that the constitution of interstellar dust in external galaxies is believed to differ significantly from the MW. Dust build-up and evolution indeed depend on the particular *Star Formation History* (SFH) of each galaxy. In particular, the metallicity, Z, appears to be one of the most important factors.[12] This parameter, Z, quantifies the cumulated elemental enrichment of a system. To properly interpret observations of galaxies, we thus need to understand how the dust properties vary as a function of Z. Yet, as we have seen, contemporary dust models,[27,36] that are used to provide such an interpretation, are exclusively constrained by observations of the MW, a system with a narrow Z range around the Solar value, $Z_\odot$. We are therefore biased by the particular properties of the MW when modeling the dust SED of other galaxies. This bias especially questions our ability to accurately understand nearby dwarf galaxies and early Universe galaxies for which the metal enrichment is expected to be low.

2.1 The need for a fully-constrained extragalactic dust model

Arguably, no properly-constrained dust model of external galaxies currently exists. This is because there is a deficit of observational constraints. Several teams have fitted the extinction curves of the Magellanic Clouds with realistic optical properties and a range of sizes.[37–39] There are however strong degeneracies between these optical properties and the size distribution. Contemporary dust models for the Milky Way address this degeneracy by combining the constraints coming from the IR emission, the UV-NIR extinction, and elemental depletions[36,40–42] and more recently the polarization.[27,28] The mixing of physical conditions along the sightline and within the telescope beam indeed renders the SED degenerate. For instance, if we are observing a region where there is a gradient of *InterStellar Radiation Field* (ISRF), we will not be able to distinguish an over-abundance of small grains from the spread due to the variation of the equilibrium temperatures of large grains (*e.g.* Fig. 3 of Galliano *et al.*, 2018[1]). This is why dust models are calibrated on observations of the diffuse ISM of the MW. The low optical depth of this medium ($A(\mathrm{V}) \simeq 0.1$ for $N(\mathrm{H\,I}) \simeq 2 \times 10^{20}$ H/cm^2, at $Z = Z_\odot$) ensures that the grains will be uniformly illuminated by the average ISRF. It is possible to build the observed SED of the diffuse ISM of the MW, by averaging the high Galactic latitude fluxes given by IRAS, COBE and *Planck*. This is however not yet possible in external galaxies. IRAS, COBE and *Planck* did not sufficiently resolve galaxies to allow the extraction of their diffuse ISM emission, without contaminations by denser clouds. And other observatories with a finer angular resolution, such as *Spitzer* and *Herschel*, were not sensitive enough (*Herschel* could barely go below $N(\mathrm{H\,I}) \simeq 10^{22}$ H/cm^2).

The good angular resolution and the exceptional sensitivity of PRIMA over the whole *Mid-InfraRed-to-Far-InfraRed* (MIR-to-FIR) window gives us a way to palliate this problem, without having to resort to combining observations that trace different scales (also called *feathering*).[44] The two closest galaxies, the *Large and Small Magellanic Clouds* (LMC & SMC; distances: $d_{\mathrm{LMC}} = 50$ kpc and $d_{\mathrm{SMC}} = 60$ kpc; metallicities: $Z_{\mathrm{LMC}} = 1/2\ Z_\odot$ and $Z_{\mathrm{SMC}} = 1/5\ Z_\odot$; Fig. 1) are ideal targets. We will be able to resolve regions of $\simeq 10$ pc size at $\lambda = 250\ \mu$m. With the addition of already estimated elemental depletions and extinction curves,[8,45] the well-characterized broad-band SED of their diffuse emission per H atom will allow us to build the first properly-constrained extragalactic, non-Solar metallicity, dust models.

2.2 *Possible observing strategy*

To measure the MIR-to-FIR SED of the diffuse ISM of the LMC and SMC, we need to make deep maps of these two galaxies in all available bands. In addition, FIR measures of the polarization fraction are important to constrain the grain composition.[46] We could use PRIMAger, to measure both the total power and the polarization fraction (Table 1).

1. We could make large maps of the LMC ($12° \times 12°$) and SMC ($8° \times 6°$) with PRIMAger at the 4 long-wavelength bands.

2. To keep the observing time under a reasonable duration, we could also make smaller maps ($0.2° \times 0.2°$) of a diffuse region in each galaxy, in each of the short-wavelength bands, as confusion is less problematic in the MIR.

3. Similarly, detecting the polarization fraction would be prohibitive over the whole galaxies, but could be feasible for the same $0.2° \times 0.2°$ region with a deeper scanning time.

This observing strategy is summarized in Table 1. Taking advantage of the parallel mode, this science case could be fully executed in a total of $235 + 325 + 78 + 235 = 963$ hours. If we do not aim detecting the polarization intensity at 96 μm, this total observing time would be reduced to $235 + 190 + 78 + 190 = 693$ hours.

The *Spitzer* and *Herschel* maps of the Magellanic clouds are good.[47–49] However, they are not deep enough for this science case. Besides, PRIMA will provide a finer spectral sampling. The main challenge of this science case is the confusion with the diffuse dust emission of the MW

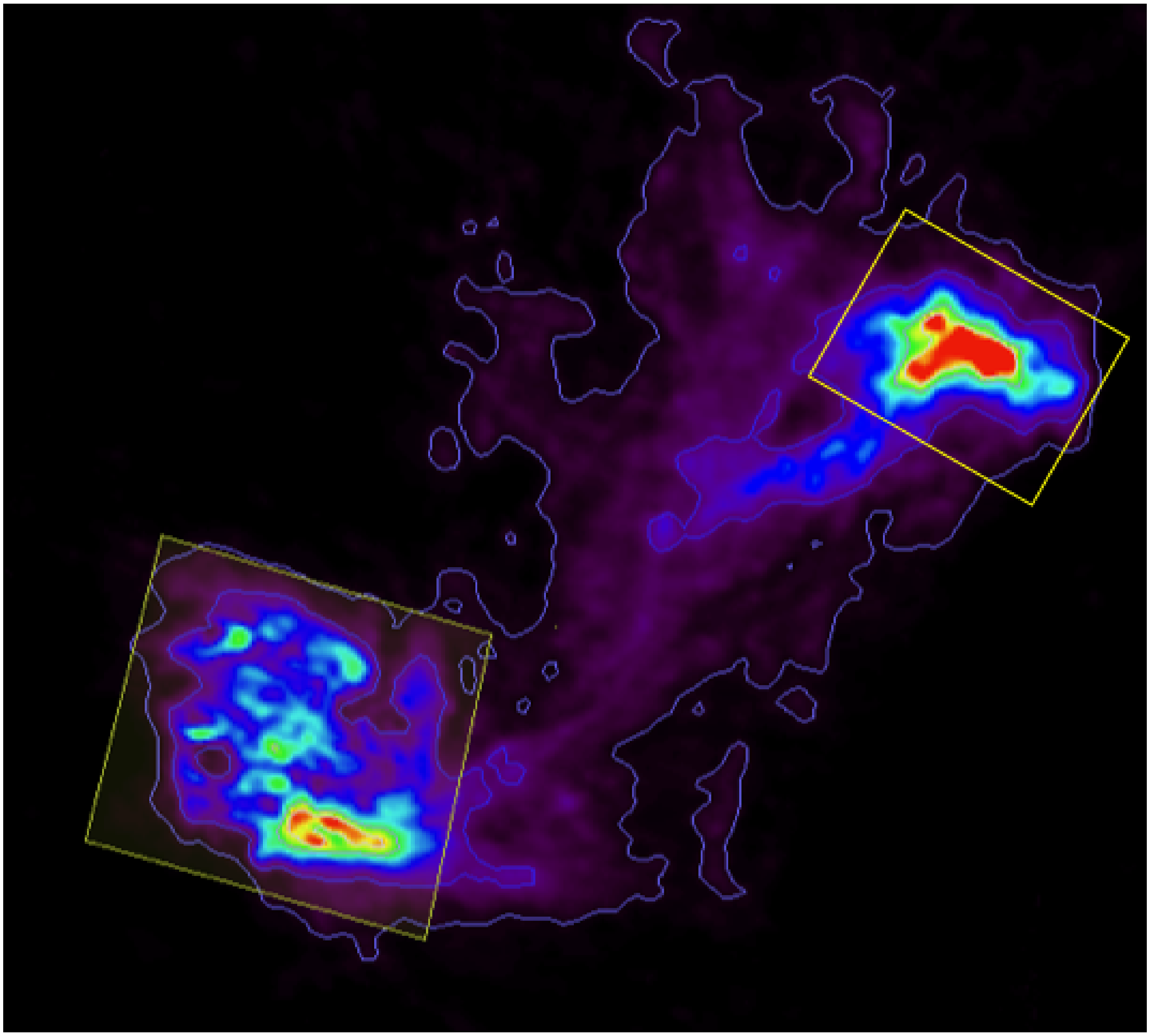

Fig 1 H I map of the LMC / SMC.[43] The contours correspond to $N(\mathrm{H\,I}) = 10^{20}$ H/cm^2 and $N(\mathrm{H\,I}) = 2 \times 10^{20}$ H/cm^2. The yellow rectangles are areas covering most of the H I emission of both sources (LMC: $12° \times 12°$; SMC: $8° \times 6°$).

Table 1 Sensitivity and observing time estimates of the diffuse ISM of the Magellanic Clouds (Sect. 2). Lines highlighted in grey are observations we could drop to keep the observing time under control. Taking advantage of the parallel mode observations, each one of the four blocks of this table represents one single observation, where all the bands are integrated in parallel.

PRIMAger band	**Field**	**Sensitivity**	**Integration time**
LMC (long-wavelength total power)			
PPI1 96 μm (total power)	$12° \times 12°$	3.91 MJy/sr	235 hours
PPI2 126 μm (total power)	$12° \times 12°$	5.12 MJy/sr	79 hours
PPI3 172 μm (total power)	$12° \times 12°$	4.49 MJy/sr	55 hours
PPI4 235 μm (total power)	$12° \times 12°$	3.00 MJy/sr	68 hours
LMC (short-wavelength & long-wavelength polarization)			
PHI1 24–45 μm	$0.2° \times 0.2°$	0.21 MJy/sr	190 hours
PHI2 45–84 μm	$0.2° \times 0.2°$	1.20 MJy/sr	1.74 hours
PPI1 96 μm (polarization)	$0.2° \times 0.2°$	3.91×0.1 MJy/sr	325 hours
PPI2 126 μm (polarization)	$0.2° \times 0.2°$	5.12×0.1 MJy/sr	110 hours
PPI3 172 μm (polarization)	$0.2° \times 0.2°$	4.49×0.1 MJy/sr	77 hours
PPI4 235 μm (polarization)	$0.2° \times 0.2°$	3.00×0.1 MJy/sr	92 hours
SMC (long-wavelength total power)			
PPI1 96 μm (total power)	$8° \times 6°$	3.91 MJy/sr	78 hours
PPI2 126 μm (total power)	$8° \times 6°$	5.12 MJy/sr	26 hours
PPI3 172 μm (total power)	$8° \times 6°$	4.49 MJy/sr	19 hours
PPI4 235 μm (total power)	$8° \times 6°$	3.00 MJy/sr	23 hours
SMC (short-wavelength & long-wavelength polarization)			
PHI1 24–45 μm	$0.2° \times 0.2°$	0.21 MJy/sr	190 hours
PHI2 45–84 μm	$0.2° \times 0.2°$	1.20 MJy/sr	1.74 hours
PPI1 96 μm (polarization)	$0.2° \times 0.2°$	3.91×0.1 MJy/sr	325 hours
PPI2 126 μm (polarization)	$0.2° \times 0.2°$	5.12×0.1 MJy/sr	110 hours
PPI3 172 μm (polarization)	$0.2° \times 0.2°$	4.49×0.1 MJy/sr	77 hours
PPI4 235 μm (polarization)	$0.2° \times 0.2°$	3.00×0.1 MJy/sr	92 hours

and with the cosmic infrared background. The redundancy provided by a large number of pixels towards many sightlines is the key to subtract these contaminations. This is why we need to map large areas to allow us using a statistical decomposition method.[50]

2.3 *Assumptions*

The flux sensitivities in Table 1 have been estimated using the THEMIS dust model[36] (Appendix A), with the following assumptions.

- The ISRF intensity appears to be higher in the Magellanic clouds than in the Milky Way, because of the presence of a higher fraction of young stars and a lower ISM opacity due to the lower dust-to-gas mass ratio.[51] Galliano *et al.* (2011)[51] showed that $U \simeq 3.5$ in the LMC, and $U \simeq 8$ in the most diffuse sightlines. To remain conservative, we assume $U = 3$.

- We aim to reach the equivalent of $N(H) = 2\times10^{20}$ H/cm^2 in the MW. At first approximation, the emission and the *dust* column density both scale with Z (Appendix A). We should thus scale the emission of the model by $Z/Z_\odot$. However, we are interested in the emission of an optically thin medium ($A(V) \simeq 0.1$). This $A(V) \simeq 0.1$ will be reached at a $Z_\odot/Z$ times higher column density than in the MW. Z therefore cancels out in this estimate and we simply need to use the MW model with $N(H) = 2 \times 10^{20}$ H/cm^2.

3 Surveying the Mineralogical Diversity of the ISM

Outside the diffuse ISM, where we are looking at denser regions of the MW and nearby galaxies, the dust model constraints discussed in Sect. 2 become more ambiguous to interpret, because of the mixing of physical conditions along the sightline. In addition, extinction and depletions become more difficult to obtain, as it becomes more difficult to detect background sources in front of dense clouds. We thus need to find other ways to study the dust properties in denser regions.

3.1 *The need for a deep extragalactic mineralogical survey*

In particular, the chemical composition and structure of dust grains is still widely unknown. We have approximate indirect constraints coming from the elemental depletions, in the diffuse ISM, and from the detection of a few broad features. The large uncertainty of dust models however is a consequence of our ignorance of this composition and structure. For instance, Zubko *et al.* (2004)[40] assume it is made of $4.6\,\%$ Polycyclic Aromatic Hydrocarbons (PAHs), $16.4\,\%$ of graphite and $79\,\%$ of amorphous silicates; Compiègne *et al.* (2011)[52] assume it is made of $7.7\,\%$ of PAHs, $15.8\,\%$ of amorphous carbon and $76.5\,\%$ of amorphous silicates; Jones *et al.* (2017)[36] assume it is made of $31.1,\%$ of partially hydrogenated amorphous carbon and $68.9\,\%$ of amorphous silicates (forsterite and enstatite in equal proportions) with hydrogenated amorphous carbon mantles and Fe/FeS inclusions; Hensley & Draine (2022)[27] assume it is made of $5\,\%$ PAHs and $95\,\%$ of a mash-up of silicate, hydrocarbons, iron and various oxides. This uncertainty is the main limitation of dust studies and of dust-based diagnostics of the physical conditions. This is also the limitation in the precision of gas-physics simulations, such as *PhotoDissociation Region* (PDR) models.[53]

The most straightforward way to more precisely constrain the dust composition would be to look for solid-state features. This is the only way to unambiguously identify a particular chemical composition. The MIR range is potentially the richest domain as it is where the vibrational modes of chemical bonds are located. For instance, we know that interstellar silicates are mostly amorphous.[54] However, precisely knowing this fraction and the way it varies with the physical conditions (radiation field, gas density and metallicity) would provide invaluable constraints on dust evolution. Another puzzle is that there is too much depleted oxygen in the ISM, compared to what we can put in silicates. It is thus possible that a fraction of the dust is in the form of various oxides (*e.g.* Al_2O_3, $CaCO_3$, *etc.*) or organic carbonates.[55] The bands of these compounds may have eluded previous spectroscopic surveys. Finally, recent X-ray investigations of the dust chemical composition in our Galaxy suggest that Mg-rich amorphous pyroxene represents the largest fraction of dust (about $70\,\%$ on average[56]). This fraction may change with environments and amorphous pyroxenes can be studied through their MIR-to-FIR features as well.

3.2 Possible observing strategy

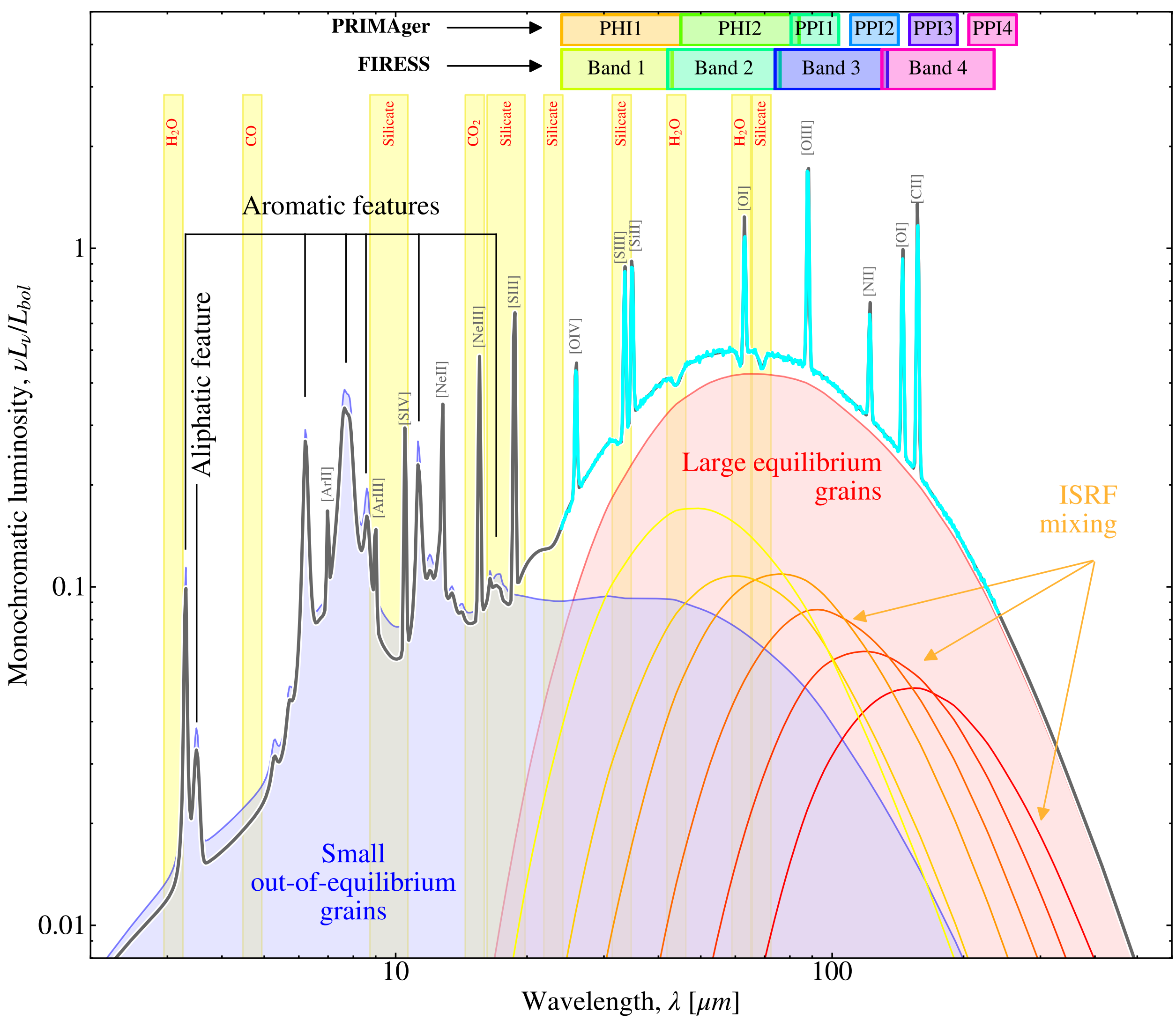

Fig 2 Typical SED of a star-forming region simulated with the THEMIS model.[36] The cyan line is a simulated $R = 150$ FIRESS spectrum (100σ). We show a few absorption features from crystalline silicates and ices,[57] and the brightest gas lines.[58]

Low *spectral resolution* (R), high *signal-to-noise ratio* (S/N) observations over the whole MIR-to-FIR range would give us access to a wealth of features (Fig. 2). However, such spectra were only obtained in the past by combining ISOSWS and ISOLWS,[59] with a poor sensitivity, a poor spatial resolution and stitching problems. This is a domain where PRIMA will particularly pioneer. We could map star-forming regions of different metallicities, such as in the LMC and SMC. It would be important to obtain maps in order to understand how these features vary with the distance from the central cluster. This would highlight the role of photo-processing as well as the role of mantle growth. We could be looking for both emission and absorption features. However, the emission features come primarily from small grains or large hot grains. They might not represent the bulk of the dust mass. This is why absorption features are preferred. This is also why we would need to target star-forming regions, so that we have a strong MIR background.

We could thus use FIRESS to perform $R \simeq 150$ spectral maps of a sample of 20 nearby extragalactic star-forming regions ($\simeq 20' \times 20'$), in the Magellanic clouds. Taking advantage of the parallel observations of bands 1 and 3, and of bands 2 and 4, 20 regions could be mapped in 996 hours (Table 2).

Table 2 Spectroscopic time estimates for the mineralogical studies of Magellanic star-forming regions.

Band [μm]	**Fields**	**Sensitivity [W/m^2]**	**Time [hours]**
		LMC	
Band 1	$12 \times (20' \times 20')$	8.8×10^{-17}	180
Band 2	$12 \times (20' \times 20')$	3.2×10^{-16}	13
Band 3	$12 \times (20' \times 20')$	7.0×10^{-16}	1.2
Band 4	$12 \times (20' \times 20')$	5.4×10^{-16}	0.7
		SMC	
Band 1	$8 \times (20' \times 20')$	3.5×10^{-17}	748
Band 2	$8 \times (20' \times 20')$	1.3×10^{-16}	55
Band 3	$8 \times (20' \times 20')$	2.8×10^{-16}	4.9
Band 4	$8 \times (20' \times 20')$	2.2×10^{-16}	3.1

3.3 Assumptions

The flux sensitivity has been estimated using the `THEMIS` dust model[36] with the following assumptions (Appendix A).

- We assume a radiation field intensity of $U = 35$ and a Hydrogen column density of $N(\mathrm{H\,I}) = 10^{22}$ H/cm^2. This corresponds approximately to the extended parts of the star-forming regions of the LMC.[51]
- We would require a high S/N ($\simeq 100$), because the goal is not so much to detect the intensity of a feature, but to unambiguously measure it. These features are usually weak and broad, we thus need to make sure that they are not diluted in the continuum.
- The sizes ($20' \times 20'$) are those of typical star-forming regions in the LMC / SMC (N 11, N 66, *etc.*).

4 Disentangling the Effects of Metallicity and Star Formation Activity on the Dust Properties

Our understanding of both *local* (*i.e.* at the scale of clouds) and *global* or *cosmic* (*i.e.* at the scale of galaxies) dust evolution relies primarily on the empirical evidence that the grain properties are changing with the physical conditions.[12,60–62] To that purpose, we can consider different targets as snapshots of galaxy evolution at different stages. As mentioned in Sect. 1, the most used environmental parameter to quantify the evolution of a galaxy is its metallicity, Z, as it traces the cumulated elemental enrichment of its ISM. However, different SFHs, and thus different evolutionary paths, can lead to the same Z at a given age. Consequently, we often face a degeneracy between the effects of metal enrichment and star formation activity, when attempting to interpret dust evolution trends.

4.1 *The necessity to obtain IR observations of quiescent low-metallicity galaxies*

This degeneracy is illustrated by Fig. 3, showing the evolution of the fraction of small amorphous carbon grains as a function of Z and average starlight intensity, $\langle U \rangle$, in individual galaxies.[12] It ambiguously suggests that the evolution of these small grains could be driven either by Z or by the *specific Star Formation Rate* (sSFR). This is because the low-Z galaxies detected with Herschel are primarily actively star-forming. This selection effect therefore results in a correlation between these two parameters in our sample, and we are unable to understand which one is fundamental. This degeneracy is encountered when looking at other quantities, too.

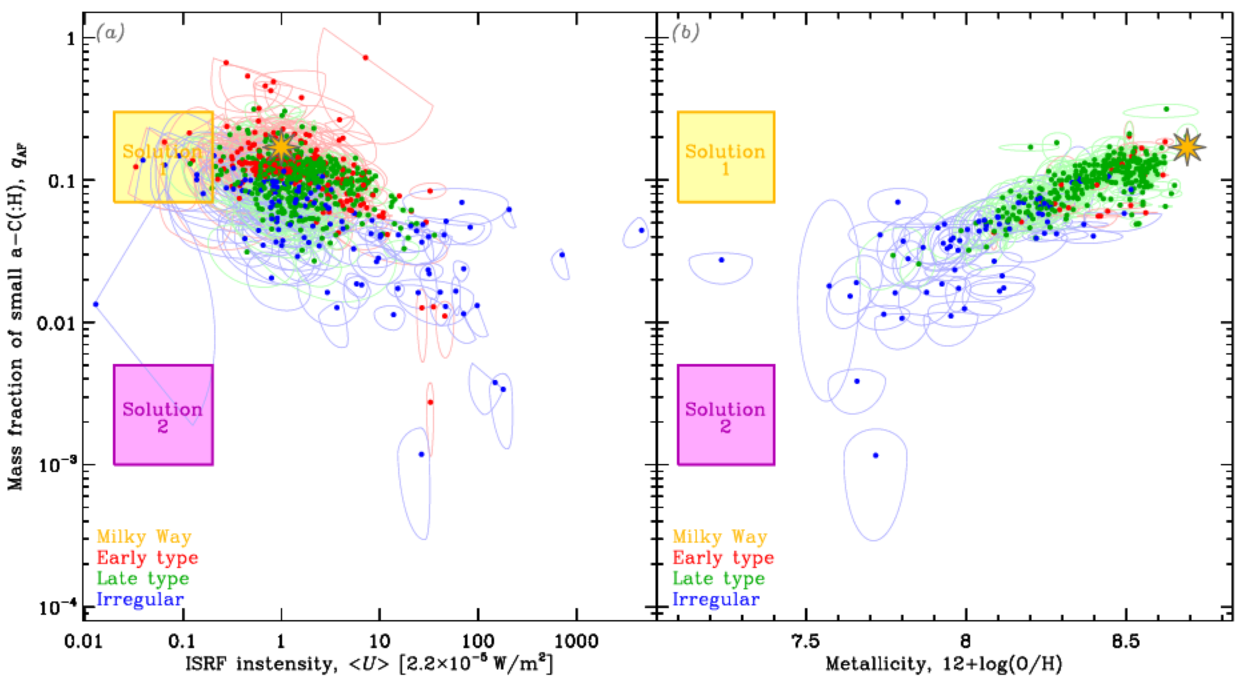

Fig 3 The potential of quiescent very-low-Z galaxies. We show the mass fraction of small amorphous carbon grains, $q_{\rm AF}$, as a function of starlight intensity, $\langle U \rangle$ (panel *a*), and metallicity. Z (panel *b*). Each point corresponds to one galaxy of the Galliano *et al.* (2021)[12] sample. We have added two hypothetical observations of a quiescent very-low-Z galaxy (solutions 1 and 2). Such observations would break the degeneracy between Z and $\langle U \rangle$, as they can not be consistent with both trends.

There is however a population of low sSFR, low-Z galaxies, distinct from those in our sample.[63] Deriving the dust properties in these objects would thus allow us to break this type of degeneracy, as these sources would necessarily appear as a distinct branch in one of the two panels of Fig. 3 (solution 1 or solution 2). In addition, learning more about these local galaxies is interesting for the interpretation of deep surveys, as they probe the faint end of the luminosity function. These objects are also local analogs to distant primordial galaxies. Herschel was successful in detecting a few very low-Z star-forming objects (essentially I Zw 18 and SBS 0335-052). PRIMA could observe a sample of 100 nearby very low-Z galaxies (1/10 to 1/30 $Z\odot$; typical size $2' \times 2'$). For instance, the ALFALFA $[\mathrm{H\,I}]_{21\,\mathrm{cm}}$ survey[64] contains hundreds of galaxies with $M(\mathrm{H\,I}) < 10^8\ M_\odot$ and dozens with $M(\mathrm{H\,I}) < 10^7\ M_\odot$. Among them, several have been well observed in stellar and ionized gas tracers: the 12 sources from the SHIELD sample;[65] the very low surface density, nearby object, Leo P;[66] the most metal-poor gas-rich galaxy known to date, AG 198691.[67] We also need more statistics in the low-Z / high-sSFR branch. We thus need to explore the whole sSFR range at very low Z.

4.2 Possible observing strategy

The unprecedented sensitivity of PRIMA should allow us to detect these objects at all IR wavelengths. Obtaining the well-sampled IR SED of these objects would allow us to understand the role of Z and sSFR in shaping the dust properties at early stages. Ideally, we would like to map this galaxy sample with all PRIMAger bands. We would also need low-resolution spectral maps, with FIRESS, to better constrain the shape of the continuum in different regions. Mapping 100 of these sources would take less 31 hours (Table 3), and $R \simeq 150$ spectral mapping (except maybe in band 1) would take less than 100 hours (Table 4).

4.3 Assumptions

We do not know much about the ISM properties of low surface brightness galaxies. Most of these objects have been detected only through their stellar emission or $[\mathrm{H\,I}]_{21\,\mathrm{cm}}$ line. The flux sensitivity has been estimated using the `THEMIS` dust model,[36] assuming a typical $U = 3$, similar to Sect. 2, and aiming for an H column density of $N(\mathrm{H\,I}) = 10^{21}$ H/cm^2.

Table 3 PRIMAger time estimates for the quiescent low-metallicity sample.

Band [μm]	Fields	Sensitivity [MJy/sr]	Time [hours]
PHI1	$100 \times (2' \times 2')$	0.85	31
PHI2	$100 \times (2' \times 2')$	4.9	0.3
PPI1	$100 \times (2' \times 2')$	16	< 0.1
PPI2	$100 \times (2' \times 2')$	21	< 0.1
PPI3	$100 \times (2' \times 2')$	18	< 0.1
PPI4	$100 \times (2' \times 2')$	12	< 0.1

5 Self-Consistently Probing the Dust Properties and the ISM Structure of Nearby Galaxies

5.1 A gas and dust multiphase model

The degeneracies we face when modeling the dust SEDs of dense regions, and that we have discussed in this paper, originate in our inability to separate the effects due to the variation of the

Table 4 FIRESS time estimates for the quiescent low-metallicity sample. The line highlighted in grey is an observation we could drop to keep the observing time under control.

Band [μm]	Fields	Sensitivity [W/m^2/sr]	Time [hours]
Band 1	$100 \times (2' \times 2')$	6.9×10^{-19}	595
Band 2	$100 \times (2' \times 2')$	1.7×10^{-19}	97
Band 3	$100 \times (2' \times 2')$	1.4×10^{-17}	0.6
Band 4	$100 \times (2' \times 2')$	2.6×10^{-17}	0.1

microscopic grain properties and those due to the macroscopic topology of the ISM. This problem has been addressed, concerning the gas, by state-of-the-art models, where a large number of lines could be used to constrain both the physical conditions of the ISM and its topology in galaxies.[68] This has been possible because atomic physics is more precisely known than dust physics. The fact that different ions have a wide range of critical densities allows us to use a few well-chosen lines to characterize the main phases of the ISM. The knowledge of the average structure of the ISM and of the stellar distribution, provided by the lines, could thus be used as an *a priori* to model the dust properties. Yet, obtaining at the same time a well-sampled SED and the intensity of the main IR gas lines is observationally challenging and has been achieved in only a handful of sources, most of the time for a single pointing.

5.2 *Possible observing strategy*

The combined MIR-to-FIR photometric and spectroscopic capability of PRIMA opens the window to obtaining consistent spatially-resolved maps of the total dust and multiphase gas properties in extragalactic regions. Such spectra were only obtained in the past by combining ISOSWS and ISOLWS,[59] but with a poor sensitivity, a poor spatial resolution and stitching problems. If we have only a few broadband observations, scattered over the whole IR domain, as it is usually the case, we are unable to solve the degeneracy discussed above.[1] The unique feature brought by PRIMA will be consistent maps of the brightest far-IR lines, with the well-sampled dust continuum.

We would observe a sample of nearby galaxies, both in narrow-band imaging and low-resolution spectroscopy. We do not need to reach the lowest emission of these objects, but we would need to have contiguous maps, in order to understand the spatial variations. Such combined dust-gas maps could be modeled using `Cloudy`[69] and the `Meudon PDR code`[70] for the gas, a dust evolution model such as `THEMIS`[36] for the dust and a radiative transfer code such as SOC.[71] In addition, recent JWST observations suggest that the PAH emission and the star-formation is enhanced in filamentary structures, which are supposed to have been created by shocks.[72] The numerous shock tracers in the FIRESS spectral range could thus be used to understand the heating of the gas in addition to PDRs, using the Paris-Durham shock model.[73] We could observe 30 disk galaxies ($20' \times 20'$) and 100 low-metallicity galaxies ($2' \times 2'$; 1/10 to 1/3 $Z_\odot$) in order to be able to build an evolutionary sequence of the dust properties. The outer regions of face-on disk galaxies can also have a low metallicity,[74,75] and thus complement our sampling of this parameter range. We would observe this galaxy sample with all PRIMAger bands, and with FIRESS at low spectral resolution. This could be done in $\simeq 860$ hours (Tables 5 – 6).

5.3 *Assumptions*

The flux sensitivity has been estimated using the THEMIS model[36] (Appendix A).

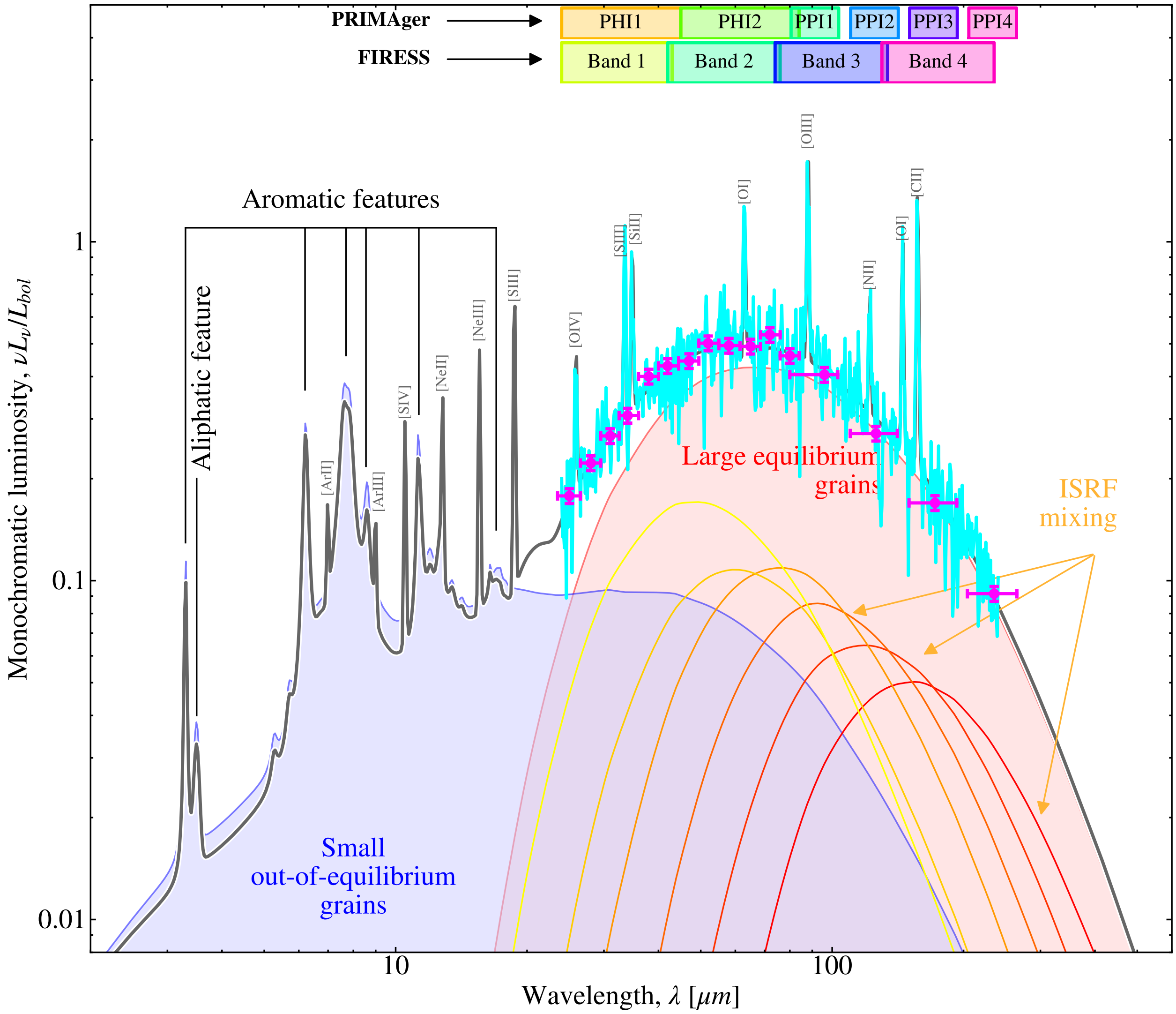

Fig 4 Typical SED of a star-forming region with the brightest gas lines. The magenta error bars correspond to a simulated PRIMAGER broad-band spectrophotometry with $R \simeq 4$ for PPI and $R \simeq 10$ for PHI (10σ), and the cyan line is a $R \simeq 150$ simulated FIRESS spectrum (5σ).

Table 5 PRIMAger time estimates for the Sect. 5 science case.

	Sensitivity	**Disks**	**Dwarfs**
PHI1	0.85 MJy/sr	628 hours	226 hours
PHI2	4.91 MJy/sr	5.8 hours	2.1 hours
PPI1	14.9 MJy/sr	0.3 hours	$<$ 0.1 hours
PPI2	21.0 MJy/sr	$<$ 0.1 hours	$<$ 0.1 hours
PPI3	18.4 MJy/sr	$<$ 0.1 hours	$<$ 0.1 hours
PPI4	12.3 MJy/sr	$<$ 0.1 hours	$<$ 0.1 hours

Table 6 FIRESS time estimates for the Sect. 5 science case.

		Sensitivity	Disks	Dwarfs
Band 1	[S III]$_{33.48\mu m}$	1.15×10^{-16} W/m^2	0.4 hours	0.2 hours
	[Si II]$_{34.82\mu m}$	4.19×10^{-17} W/m^2	3.3 hours	1.2 hours
Band 2	[O I]$_{63\mu m}$	5.98×10^{-16} W/m^2	<0.1 hours	<0.1 hours
Band 3	[O III]$_{88\mu m}$	1.69×10^{-15} W/m^2	<0.1 hours	<0.1 hours
	[N II]$_{122\mu m}$	3.82×10^{-17} W/m^2	<0.1 hours	<0.1 hours
Band 4	[O I]$_{145\mu m}$	1.02×10^{-16} W/m^2	<0.1 hours	<0.1 hours
	[C II]$_{158\mu m}$	2.94×10^{-15} W/m^2	<0.1 hours	<0.1 hours

- We have assumed $U = 3$ and $N(\mathrm{H\,I}) = 10^{21}$ H/cm^2 in Table 5. This corresponds to the typical extended emission of disk galaxies found in the DustPedia sample.[76,77] This is however not the most diffuse emission of the galaxy, but this value is sufficient for the present science case, where we are interested in the multiphase nature of the ISM.

- The fine-structure lines are all bright. In addition, we do not need to spectrally resolve them. Low-resolution spectroscopy should thus be sufficient to measure their intensity. We have estimated the line intensity in Table 6, by assuming they are proportional to the total IR luminosity. The proportionality factor of each line is the average of the sample in Cormier *et al.* (2019).[58]

6 Summary and Conclusion

To summarize our thoughts, the unprecedented sensitivity of PRIMA will allow us to conduct a few large programs of observations (less than 3000 hours) that should give us key constraints to unlock our understanding of interstellar dust evolution.

1. The exceptional sensitivity of PRIMA will allow us to get deep-enough maps of external galaxies to detect their most diffuse ISM over the whole MIR-to-FIR window. This is essential to build rigorously-constrained extragalactic dust models (Sect. 2).

2. PRIMA's unique $\lambda = 24 - 325$ μm continuous $R = 150$ spectroscopic capability will allow us to detect faint solid-state features that are a key to refining our understanding of the chemical composition and structure of interstellar grains (Sect. 3).

3. PRIMA's sensitivity will also allow us to measure the FIR SED of quiescent low-metallicity galaxies and thus understand which grain properties are primarily determined by the elemental evolution of the ISM and which one are controlled by the star-formation activity (Sect. 4).

4. Finally, the continuous spectroscopic capability of PRIMA will allow us to map, within the same observations, the MIR-to-FIR SED and numerous gas lines. This will allow us to constrain self-consistent multiphase ISM models, and thus solve the degeneracies between the microscopic grain properties and their macroscopic topology (Sect. 5).

These science cases show that PRIMA is a key facility to progress both in our understanding of the physics of the ISM and of galaxy evolution. Our poor knowledge of the dust properties, a consequence of their complexity, is already the main limitation of the current models of the

ISM[53] and galaxy evolution.[2] Without the observations proposed in this paper, our progress in the major open questions listed in Sect. 1 would be greatly limited. The FIR range is crucial to these topics and the possible non-selection of PRIMA by NASA would close the FIR window for several decades.

Appendix A: PRIMA Time Estimation

A.1 *Surface brightness estimates*

Our surface brightness estimates are based on the THEMIS model.[36] We use it to estimate the surface brightness, I_ν, corresponding to the thermal dust emission, for a given Hydrogen column density, $N_{\rm H}$, and ISRF intensity, U.

The ISRF of the Solar neighborhood[78] is simply scaled by the dimensionless parameter U,[41] $U = 1$ being the value used for the diffuse Galactic ISM. The effect of this parameter on the dust surface brightness is non trivial (Fig. 5).

The dust column density is assumed to scale linearly with metallicity, Z: $N(\text{dust}) = N(\text{H}) \times m_{\rm H} \times Y_{\rm H} \times Z$, where $Y_{\rm H} \equiv M_{\rm dust}/M_{\rm H} = 7.4 \times 10^{-3}$ and $m_{\rm H}$ is the mass of an H atom.[36] The dust surface brightness subsequently scales linearly with $N(\text{dust})$.

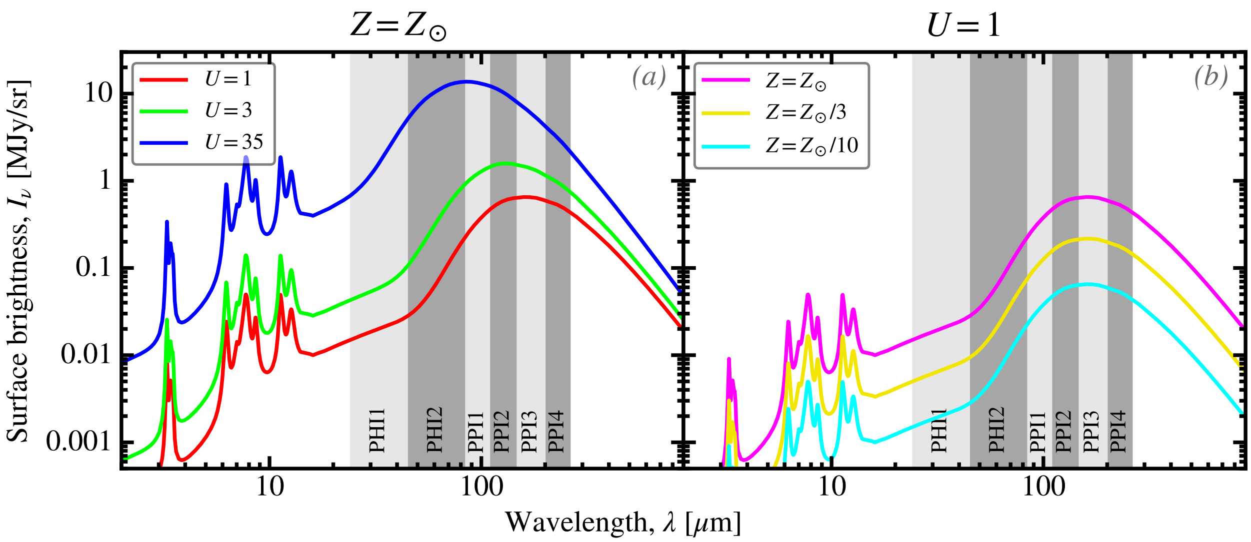

Fig 5 Both panels show the surface brightness of the THEMIS dust model, varying the ISRF intensity, U (panel *a*), and varying the metallicity, Z (panel *b*). All these curves correspond to the very diffuse ISM, $N(\text{H}) = 10^{20}$ H/cm^2.

A.2 *Observing time*

Our observing strategy is based on the PRIMA instrument characteristics and sensitivities that were available in December 2024 at: https://prima.ipac.caltech.edu/page/instruments.

PRIMAger: the sensitivities, I_ν^0 and P_ν^0, are summarized in Table 7. We thus estimate our observing times, including overheads, for a mapping area A as:

$$t_{\text{obs}}^{\text{total}} = \left(\frac{I_\nu^0}{I_\nu}\right)^2 \times \left(\frac{N_\sigma}{5}\right)^2 \times \frac{A}{1^{\circ 2}} \times 10 \text{ hours} \quad (1)$$

$$t_{\text{obs}}^{\text{pola}} = \left(\frac{P_\nu^0}{f_{\text{pol}} I_\nu}\right)^2 \times \left(\frac{N_\sigma}{5}\right)^2 \times \frac{A}{1^{\circ 2}} \times 10 \text{ hours}, \quad (2)$$

where N_σ is the number of σ we aim to reach and $f_{\text{pol}} = 10\,\%$ is the estimated polarization fraction.

FIRESS: the observing time for measuring the integrated intensity, I, of a line centered at λ, at level N_σ, mapped over an area A, is:

$$t_{\text{obs}}^{\text{low-res}} = \left(\frac{3 \times 10^{-19} \text{ W/m}^2}{I}\right)^2 \times \left(\frac{N_\sigma}{5}\right)^2 \times \frac{A}{100'^2} \times \begin{cases} 800 \text{ hours} & \text{for } 24\ \mu\text{m} < \lambda < 75\ \mu\text{m} \\ \left(\dfrac{\lambda}{100\ \mu\text{m}}\right)^{-1.68} \times 336 \text{ hours} & \text{for } 75\ \mu\text{m} < \lambda < 235\ \mu\text{m} \end{cases} \quad (3)$$

Table 7 PRIMAger extended source sensitivities for a 5σ background-subtracted 1 square degree map observed during 10 hours.

	PHI1	**PHI2**	**PPI1**	**PPI2**	**PPI3**	**PPI4**
Total power, I_ν^0 [MJy/sr]	4.5	2.5	1.58	1.20	0.88	0.65
Polarized intensity, P_ν^0 [MJy/sr]	...	...	2.23	1.70	1.25	0.91

Table 8 FIRESS low-resolution parameters.

	Band 1	**Band 2**	**Band 3**	**Band 4**
Wavelength range	24–43 μm	42–76 μm	74–134 μm	130–235
Wavelength sampling	0.23 μm	0.41 μm	0.73 μm	1.29 μm
Slit width, $W(\lambda)$	7.6″	7.6″	12.7″	22.9″

Disclosures

The authors do not have any conflict of interest to disclose.

Code, Data, and Materials Availability

All the simulations in this paper were performed using the `THEMIS` dust model that can be freely downloaded from https://www.ias.u-psud.fr/DUSTEM/.

Acknowledgments

We thank our two anonymous referees for their insightful comments. This work is supported by the French National Research Agency under the contract WIDENING ANR-23-ESDIR-0004, as well as by the Programme National "Physique et Chimie du Milieu Interstellaire" (PCMI) of CNRS/INSU, with INC and INP, and the "Programme National Cosmologie et Galaxies" (PNCG) of CNRS/INSU, with INP and IN2P3, both programs being co-funded by CEA and CNES.

References

1 F. Galliano, M. Galametz, and A. P. Jones, "The Interstellar Dust Properties of Nearby Galaxies," ARA&A **56**, 673–713 (2018).

2 Y. Dubois, F. Rodríguez Montero, C. Guerra, et al., "Galaxies with grains: unraveling dust evolution and extinction curves with hydrodynamical simulations," A&A **687**, A240 (2024).

3 U. Lebreuilly, P. Hennebelle, A. Maury, et al., "Influence of protostellar outflows on star and protoplanetary disk formation in a massive star-forming clump," A&A **683**, A13 (2024).

4 M. Guélin and J. Cernicharo, "Organic Molecules in Interstellar Space: Latest Advances," Frontiers in Astronomy and Space Sciences **9**, 787567 (2022).

5 N. Ysard, M. Köhler, A. Jones, et al., "Dust variations in the diffuse interstellar medium: constraints on Milky Way dust from Planck-HFI observations," A&A **577**, A110 (2015).

6 J. Lequeux, E. Maurice, M.-L. Prevot-Burnichon, et al., "SK 143 - an SMC star with a galactic-type ultraviolet interstellar extinction," A&A **113**, L15–L17 (1982).

7 L. A. Valencic, G. C. Clayton, K. D. Gordon, et al., "Small Magellanic Cloud-Type Interstellar Dust in the Milky Way," ApJ **598**, 369–374 (2003).

8 K. D. Gordon, G. C. Clayton, K. A. Misselt, et al., "A Quantitative Comparison of the Small Magellanic Cloud, Large Magellanic Cloud, and Milky Way Ultraviolet to Near-Infrared Extinction Curves," ApJ **594**, 279–293 (2003).

9 J. Maíz Apellániz and M. Rubio, "Ultraviolet extinction toward a quiescent molecular cloud in the Small Magellanic Cloud," A&A **541**, A54 (2012).

10 K. D. Gordon, E. L. Fitzpatrick, D. Massa, et al., "Expanded Sample of Small Magellanic Cloud Ultraviolet Dust Extinction Curves: Correlations between the 2175 Å Bump, q $_{PAH}$, Ultraviolet Extinction Shape, and N(H I)/A(V)," ApJ **970**, 51 (2024).

11 K. M. Sandstrom, A. D. Bolatto, C. Bot, et al., "The Spitzer Spectroscopic Survey of the Small Magellanic Cloud (S^4MC): Probing the Physical State of Polycyclic Aromatic Hydrocarbons in a Low-metallicity Environment," ApJ **744**, 20 (2012).

12 F. Galliano, A. Nersesian, S. Bianchi, et al., "A nearby galaxy perspective on dust evolution. Scaling relations and constraints on the dust build-up in galaxies with the DustPedia and DGS samples," A&A **649**, A18 (2021).

13 C. M. Whitcomb, J. D. T. Smith, K. Sandstrom, et al., "The Metallicity Dependence of PAH Emission in Galaxies. I. Insights from Deep Radial Spitzer Spectroscopy," ApJ **974**, 20 (2024).

14 J. Roman-Duval, E. B. Jenkins, K. Tchernyshyov, et al., "METAL: The Metal Evolution, Transport, and Abundance in the Large Magellanic Cloud Hubble Program. II. Variations of Interstellar Depletions and Dust-to-gas Ratio within the LMC," ApJ **910**, 95 (2021).

15 J. Roman-Duval, E. B. Jenkins, K. Tchernyshyov, et al., "METAL: The Metal Evolution, Transport, and Abundance in the Large Magellanic Cloud Hubble Program. III. Interstellar Depletions, Dust-to-Metal, and Dust-to-Gas Ratios versus Metallicity," ApJ **928**, 90 (2022).

16 J. Roman-Duval, E. B. Jenkins, K. Tchernyshyov, et al., "METAL: The Metal Evolution, Transport, and Abundance in the Large Magellanic Cloud Hubble Program. IV. Calibration of Dust Depletions versus Abundance Ratios in the Milky Way and Magellanic Clouds and Application to Damped Lyα Systems," ApJ **935**, 105 (2022).

17 F. Galliano, S. C. Madden, A. P. Jones, et al., "ISM properties in low-metallicity environments. II. The dust spectral energy distribution of NGC 1569," A&A **407**, 159–176 (2003).

18 F. Galliano, S. C. Madden, A. P. Jones, et al., "ISM properties in low-metallicity environments. III. The spectral energy distributions of II Zw 40, He 2-10 and NGC 1140," A&A **434**, 867–885 (2005).

19 M. Galametz, S. Madden, F. Galliano, et al., "Probing the dust properties of galaxies up to submillimetre wavelengths. I. The spectral energy distribution of dwarf galaxies using LABOCA," A&A **508**, 645–664 (2009).

20 C. Bot, N. Ysard, D. Paradis, et al., "Submillimeter to centimeter excess emission from the Magellanic Clouds. II. On the nature of the excess," A&A **523**, A20+ (2010).

21 D. Paradis, J. P. Bernard, C. Mény, et al., "Far-infrared to millimeter astrophysical dust emission. II. Comparison of the two-level systems (TLS) model with astronomical data," A&A **534**, A118 (2011).

22 Planck Collaboration, P. A. R. Ade, N. Aghanim, et al., "Planck early results. XVII. Origin of the submillimetre excess dust emission in the Magellanic Clouds," A&A **536**, A17 (2011).

23 D. A. Dale, G. Aniano, C. W. Engelbracht, et al., "Herschel Far-infrared and Submillimeter Photometry for the KINGFISH Sample of nearby Galaxies," ApJ **745**, 95 (2012).

24 E. L. Fitzpatrick, D. Massa, K. D. Gordon, et al., "An Analysis of the Shapes of Interstellar Extinction Curves. VII. Milky Way Spectrophotometric Optical-through-ultraviolet Extinction and Its R-dependence," ApJ **886**, 108 (2019).

25 K. D. Gordon, G. C. Clayton, M. Decleir, et al., "One Relation for All Wavelengths: The Far-ultraviolet to Mid-infrared Milky Way Spectroscopic R(V)-dependent Dust Extinction Relationship," ApJ **950**, 86 (2023).

26 B. T. Draine, "Interstellar Dust Models and Evolutionary Implications," in Astronomical Society of the Pacific Conference Series, T. Henning, E. Grün, & J. Steinacker, Ed., Astronomical Society of the Pacific Conference Series **414**, 453–+ (2009).

27 B. S. Hensley and B. T. Draine, "The Astrodust+PAH Model: A Unified Description of the Extinction, Emission, and Polarization from Dust in the Diffuse Interstellar Medium," ApJ **948**, 55 (2023).

28 N. Ysard, A. P. Jones, V. Guillet, et al., "THEMIS 2.0: A self-consistent model for dust extinction, emission, and polarisation," A&A **684**, A34 (2024).

29 M. Palla, I. De Looze, M. Relaño, et al., "Metal and dust evolution in ALMA REBELS galaxies: insights for future JWST observations," MNRAS **528**, 2407–2427 (2024).

30 S. C. Madden, A. Rémy-Ruyer, M. Galametz, et al., "An Overview of the Dwarf Galaxy Survey," PASP **125**, 600–635 (2013).

31 K. M. Sandstrom, A. K. Leroy, F. Walter, et al., "The CO-to-H_2 Conversion Factor and Dust-to-gas Ratio on Kiloparsec Scales in Nearby Galaxies," ApJ **777**, 5 (2013).

32 A. Rémy-Ruyer, S. C. Madden, F. Galliano, et al., “Gas-to-dust mass ratios in local galaxies over a 2 dex metallicity range,” A&A **563**, A31 (2014).

33 J. Chastenet, C. Bot, K. D. Gordon, et al., “Modeling dust emission in the Magellanic Clouds with Spitzer and Herschel,” A&A **601**, A55 (2017).

34 J. Glenn, C. M. Bradford, E. Rosolowsky, et al., “Galaxy Evolution Probe,” Journal of Astronomical Telescopes, Instruments, and Systems **7**, 034004 (2021).

35 A. Moullet, T. Kataria, D. Lis, et al., “PRIMA General Observer Science Book,” arXiv e-prints **1**, arXiv:2310.20572 (2023).

36 A. P. Jones, M. Köhler, N. Ysard, et al., “The global dust modelling framework THEMIS,” A&A **602**, A46 (2017).

37 Y. C. Pei, “Interstellar dust from the Milky Way to the Magellanic Clouds,” ApJ **395**, 130–139 (1992).

38 J. C. Weingartner and B. T. Draine, “Dust Grain-Size Distributions and Extinction in the Milky Way, Large Magellanic Cloud, and Small Magellanic Cloud,” ApJ **548**, 296–309 (2001).

39 G. C. Clayton, K. D. Gordon, F. Salama, et al., “The Role of Polycyclic Aromatic Hydrocarbons in Ultraviolet Extinction. I. Probing Small Molecular Polycyclic Aromatic Hydrocarbons,” ApJ **592**, 947–952 (2003).

40 V. Zubko, E. Dwek, and R. G. Arendt, “Interstellar Dust Models Consistent with Extinction, Emission, and Abundance Constraints,” ApJS **152**, 211–249 (2004).

41 B. T. Draine and A. Li, “Infrared Emission from Interstellar Dust. IV. The Silicate-Graphite-PAH Model in the Post-Spitzer Era,” ApJ **657**, 810–837 (2007).

42 R. Siebenmorgen, J. Krełowski, J. Smoker, et al., “Dark dust and single-cloud sightlines in the ISM,” A&A **641**, A35 (2020).

43 C. Brüns, J. Kerp, L. Staveley-Smith, et al., “The Parkes H I Survey of the Magellanic System,” A&A **432**, 45–67 (2005).

44 C. J. R. Clark, J. C. Roman-Duval, K. D. Gordon, et al., “The Quest for the Missing Dust. II. Two Orders of Magnitude of Evolution in the Dust-to-gas Ratio Resolved within Local Group Galaxies,” ApJ **946**, 42 (2023).

45 K. Tchernyshyov, M. Meixner, J. Seale, et al., “Elemental Depletions in the Magellanic Clouds and the Evolution of Depletions with Metallicity,” ApJ **811**, 78 (2015).

46 V. Guillet, L. Fanciullo, L. Verstraete, et al., “Dust models compatible with Planck intensity and polarization data in translucent lines of sight,” A&A **610**, A16 (2018).

47 M. Meixner, K. D. Gordon, R. Indebetouw, et al., “Spitzer Survey of the Large Magellanic Cloud: Surveying the Agents of a Galaxy’s Evolution (SAGE). I. Overview and Initial Results,” AJ **132**, 2268–2288 (2006).

48 K. D. Gordon, M. Meixner, M. R. Meade, et al., “Surveying the Agents of Galaxy Evolution in the Tidally Stripped, Low Metallicity Small Magellanic Cloud (SAGE-SMC). I. Overview,” AJ **142**, 102 (2011).

49 M. Meixner, P. Panuzzo, J. Roman-Duval, et al., “The HERSCHEL Inventory of The Agents of Galaxy Evolution in the Magellanic Clouds, a Herschel Open Time Key Program,” AJ **146**, 62 (2013).

50 C. Auclair, E. Allys, F. Boulanger, et al., “Separation of dust emission from the cosmic infrared background in Herschel observations with wavelet phase harmonics,” A&A **681**, A1 (2024).

51 F. Galliano, S. Hony, J.-P. Bernard, et al., “Non-standard grain properties, dark gas reservoir, and extended submillimeter excess, probed by Herschel in the Large Magellanic Cloud,” A&A **536**, A88 (2011).

52 M. Compiègne, L. Verstraete, A. Jones, et al., “The global dust SED: tracing the nature and evolution of dust with DustEM,” A&A **525**, A103+ (2011).

53 M. Röllig, N. P. Abel, T. Bell, et al., “A photon dominated region code comparison study,” A&A **467**, 187–206 (2007).

54 H. W. W. Spoon, A. Hernán-Caballero, D. Rupke, et al., “The Infrared Database of Extragalactic Observables from Spitzer. II. The Database and Diagnostic Power of Crystalline Silicate Features in Galaxy Spectra,” ApJS **259**, 37 (2022).

55 A. P. Jones and N. Ysard, “The essential elements of dust evolution. A viable solution to the interstellar oxygen depletion problem?,” A&A **627**, A38 (2019).

56 I. Psaradaki, E. Costantini, D. Rogantini, et al., “Oxygen and iron in interstellar dust: An X-ray investigation,” A&A **670**, A30 (2023).

57 F. F. S. van der Tak, S. C. Madden, P. Roelfsema, et al., “Probing the Baryon Cycle of Galaxies with SPICA Mid- and Far-Infrared Observations,” PASA **35**, e002 (2018).

58 D. Cormier, N. P. Abel, S. Hony, et al., “The Herschel Dwarf Galaxy Survey. II. Physical conditions, origin of [C II] emission, and porosity of the multiphase low-metallicity ISM,” A&A **626**, A23 (2019).

59 E. Peeters, N. L. Martín-Hernández, F. Damour, et al., “ISO spectroscopy of compact H II regions in the Galaxy. I. The catalogue,” A&A **381**, 571–605 (2002).

60 F. Calura, A. Pipino, and F. Matteucci, “The cycle of interstellar dust in galaxies of different morphological types,” A&A **479**, 669–685 (2008).

61 F. Calura, F. Pozzi, G. Cresci, et al., “The dust-to-stellar mass ratio as a valuable tool to probe the evolution of local and distant star-forming galaxies,” MNRAS **465**, 54–67 (2017).

62 I. De Looze, I. Lamperti, A. Saintonge, et al., “JINGLE - IV. Dust, H I gas, and metal scaling laws in the local Universe,” MNRAS **496**, 3668–3687 (2020).

63 M. A. Lara-López, A. M. Hopkins, A. R. López-Sánchez, et al., “Galaxy And Mass Assembly (GAMA): the connection between metals, specific SFR and HI gas in galaxies: the Z–SSFR relation,” Monthly Notices of the Royal Astronomical Society: Letters **433**, L35–L39 (2013).

64 M. P. Haynes, R. Giovanelli, B. R. Kent, et al., “The arecibo legacy fast ALFA survey: The ALFALFA extragalactic h i source catalog,” The Astrophysical Journal **861**, 49 (2018).

65 J. M. Cannon, R. Giovanelli, M. P. Haynes, et al., “The Survey of H I in Extremely Low-mass Dwarfs (SHIELD),” ApJ **739**, L22 (2011).

66 R. Giovanelli, M. P. Haynes, E. A. K. Adams, et al., “ALFALFA Discovery of the Nearby Gas-rich Dwarf Galaxy Leo P. I. H I Observations,” AJ **146**, 15 (2013).

67 A. S. Hirschauer, J. J. Salzer, E. D. Skillman, et al., “ALFALFA Discovery of the Most Metal-poor Gas-rich Galaxy Known: AGC 198691,” ApJ **822**, 108 (2016).

68 D. Cormier, V. Lebouteiller, S. C. Madden, et al., “The nature of the interstellar medium of the starburst low-metallicity galaxy Haro 11: a multi-phase model of the infrared emission,” A&A **548**, A20 (2012).

69 G. J. Ferland, M. Chatzikos, F. Guzmán, et al., "The 2017 Release Cloudy," RMxAA **53**, 385–438 (2017).

70 F. Le Petit, C. Nehmé, J. Le Bourlot, et al., "A Model for Atomic and Molecular Interstellar Gas: The Meudon PDR Code," ApJS **164**, 506–529 (2006).

71 M. Juvela, "SOC program for dust continuum radiative transfer," A&A **622**, A79 (2019).

72 D. A. Thilker, J. C. Lee, S. Deger, et al., "PHANGS-JWST First Results: The Dust Filament Network of NGC 628 and Its Relation to Star Formation Activity," ApJ **944**, L13 (2023).

73 B. Godard, G. Pineau des Forêts, P. Lesaffre, et al., "Models of irradiated molecular shocks," A&A **622**, A100 (2019).

74 C. Chiappini, D. Romano, and F. Matteucci, "Oxygen, carbon and nitrogen evolution in galaxies," MNRAS **339**, 63–81 (2003).

75 K. D. Gordon, C. W. Engelbracht, G. H. Rieke, et al., "The Behavior of the Aromatic Features in M101 H II Regions: Evidence for Dust Processing," ApJ **682**, 336–354 (2008).

76 J. I. Davies, M. Baes, S. Bianchi, et al., "DustPedia: A Definitive Study of Cosmic Dust in the Local Universe," PASP **129**, 044102 (2017).

77 C. J. R. Clark, S. Verstocken, S. Bianchi, et al., "DustPedia: Multiwavelength photometry and imagery of 875 nearby galaxies in 42 ultraviolet-microwave bands," A&A **609**, A37 (2018).

78 J. S. Mathis, P. G. Mezger, and N. Panagia, "Interstellar radiation field and dust temperatures in the diffuse interstellar matter and in giant molecular clouds," A&A **128**, 212–229 (1983).

Frédéric Galliano is a staff researcher at the Department of Astrophysics of CEA Paris-Saclay. He received his MS and PhD degrees in astrophysics from the University of Paris XI in 2000 and 2004, respectively. He is the author of more than 200 journal papers. His current research interests include interstellar dust grains, and infrared and millimeter observations.

Takashi Onaka is a professor emeritus at the University of Tokyo. He received his BS, MS, and PhD degrees in astronomy from the University of Tokyo in 1975, 1977, and 1980, respectively. He is the author of more than 300 journal papers. He was the PI of Infrared Camera (IRC) on board the Japanese infrared satellite AKARI. His current research interests include interstellar dust grains and infrared observations.

Biographies and photographs of the other authors are not available.

List of Figures

List of Tables